Hyperpolarized 83 Kr and 129 Xe NMR Relaxation Measurements of Hydrated Surfaces: Implications for Materials Science and Pulmonary Diagnostics

ARTICLE *in* JOURNAL OF THE AMERICAN CHEMICAL SOCIETY · MARCH 2007

Impact Factor: 12.11 · DOI: 10.1021/ja065994t · Source: PubMed

6 AUTHORS, INCLUDING:

Galina E Pavlovskaya
University of Nottingham
47 PUBLICATIONS **427** CITATIONS
SEE PROFILE

John Repine
American University of Health Sciences
288 PUBLICATIONS **11,280** CITATIONS
SEE PROFILE

Thomas Meersmann
University of Nottingham
50 PUBLICATIONS **897** CITATIONS
SEE PROFILE

J|A|C|S
ARTICLES
Published on Web 01/23/2007

Hyperpolarized ^{83}Kr and ^{129}Xe NMR Relaxation Measurements of Hydrated Surfaces: Implications for Materials Science and Pulmonary Diagnostics

Zackary I. Cleveland,[†] Karl F. Stupic,[†] Galina E. Pavlovskaya,[†] John E. Repine,[‡] Jan B. Wooten,[§] and Thomas Meersmann*,[†]

Contribution from the Department of Chemistry, Colorado State University, Fort Collins, Colorado 80523, Webb-Waring Institute for Cancer, Aging, and Antioxidant Research, University of Colorado Health Science Center, Denver, Colorado 80262, and Philip Morris USA Research Center, Richmond, Virginia 23261

Received August 17, 2006; E-mail: Meer@MagneticResonance.US

Abstract: In this proof of principle work, a technique is introduced to study hydrated surfaces using hyperpolarized (hp) ^{83}Kr NMR spectroscopy. The longitudinal (T_1) relaxation of hp-^{83}Kr is shown to be extremely sensitive to the presence of adsorbed water on hydrophilic borosilicate and hydrophobic siliconized glass surfaces. The krypton surface relaxation is found to be largely independent of the total gas pressure applied to the studied materials, and the presented technique is therefore fairly robust. However, the relaxational properties of hp-^{83}Kr can be "tuned" by adjusting the composition of the optical pumping gas mixture. This effect may be important for practical applications such as hp-^{83}Kr MR imaging and can be achieved without sacrificing signal intensity. Complementary information to that of hp-^{83}Kr surface relaxation data can be obtained from hp-^{129}Xe relaxation measurements that are sensitive to the presence of paramagnetic surface sites. In contrast to the signal decay of hp-^{129}Xe, the longitudinal relaxation of ^{83}Kr is largely unaffected by paramagnetic impurities, and in some materials, ^{83}Kr and ^{129}Xe show comparable T_1 times that are caused by two completely different relaxation mechanisms. Finally, the relaxation times of ^{83}Kr in contact with bovine lung surfactant coated glass pores that are similar in size to mammalian alveoli are presented. The results suggest that in vivo MR studies may be feasible and could provide valuable information about changes in pulmonary surface chemistry.

Introduction

In situ and in vivo measurements of surface properties under ambient conditions impose serious experimental challenges, particularly when porous materials and surfaces within opaque media are of interest. Nuclear magnetic resonance (NMR) spectroscopy and magnetic resonance imaging (MRI) require transparency only within the radio frequency regime and can therefore probe surfaces that are obstructed from direct optical or other types of examination. This proof of principle demonstration combines hyperpolarized (hp) ^{83}Kr (11.5% natural abundance) and hp-^{129}Xe (26.4% natural abundance) NMR longitudinal relaxation (T_1) measurements to probe hydrated surfaces under near atmospheric conditions.

In the past, several NMR studies of thermally polarized krypton in materials have made use of the high nuclear spin ($S = {}^9/_2$) and the nuclear quadrupole moment ($Q = 0.26 \times 10^{-28}$ m^2) of the ^{83}Kr isotope. The ^{83}Kr NMR spectrum shows distinct splitting in the liquid crystalline phase caused by anisotropy in the environment of the dissolved krypton atoms.[1,2] The NMR line shape of ^{83}Kr obtained in zeolites is sensitive to pore dimensions, pore geometry, countercation charge, and, potentially, long-range disorder in the nanoporous materials.[3] The coherent evolution and relaxation behavior of ^{83}Kr (15.4 MHz resonance frequency at 9.4 T) in these materials are dominated by quadrupolar interactions and can therefore provide valuable information that is complementary to that obtained from the chemical shift observed in NMR spectroscopy with ^{129}Xe (110.6 MHz resonance frequency at 9.4 T and $S = {}^1/_2$).[4−6]

The nuclear spin polarization of ^{129}Xe can be increased (i.e., hyperpolarized) through rubidium vapor spin exchange optical pumping (RbSEOP)[7] by many orders of magnitude over the Boltzmann equilibrium value of thermally polarized ^{129}Xe at ambient temperature and high magnetic field strengths. Since its introduction $1{}^1/_2$ decades ago,[8] hp-^{129}Xe NMR has proven to be a powerful spectroscopic tool and is increasingly used to

[†] Colorado State University.
[‡] University of Colorado Health Science Center.
[§] Philip Morris USA Research Center.

(1) Ingman, P.; Jokisaari, J.; Diehl, P. *J. Magn. Reson.* **1991**, *92*, 163−169.
(2) Jokisaari, J.; Ingman, P.; Lounila, J.; Pukkinen, O.; Diehl, P.; Muenster, O. *Mol. Phys.* **1993**, *78*, 41−54.
(3) Horton-Garcia, C. F.; Pavlovskaya, G. E.; Meersmann, T. *J. Am. Chem. Soc.* **2005**, *127*, 1958−1962.
(4) Ito, T.; Fraissard, J. *J. Chem. Phys.* **1982**, *76*, 5225−5229.
(5) Ratcliffe, C. I. *Annu. Rep. NMR Spectrosc.* **1998**, *36*, 123−221.
(6) Springuel-Huet, M. A.; Bonardet, J. L.; Gedeon, A.; Fraissard, J. *Magn. Reson. Chem.* **1999**, *37*, S1−S13.
(7) Walker, T. G.; Happer, W. *Rev. Mod. Phys.* **1997**, *69*, 629−642.
(8) Raftery, D.; Long, H.; Meersmann, T.; Grandinetti, P. J.; Reven, L.; Pines, A. *Phys. Rev. Lett.* **1991**, *66*, 584−587.

10.1021/ja065994t CCC: $37.00

study porous materials, gas-surface interactions, surface chemistry, biomolecules, chemical reactors, and gas dynamics. Hp-^{129}Xe and hp-^{3}He have also led to exciting advances in the MR imaging of pulmonary airways and materials (see refs 9−11 for reviews).

The hyperpolarization of the ^{83}Kr nuclear spin is also possible through RbSEOP,[12−14] but the separation of hp-^{83}Kr from the paramagnetic and highly reactive rubidium vapor was not reported until the recent successful introduction of hp-^{83}Kr NMR spectroscopy[15,16] and MRI.[17] The T_1 time of hp-^{83}Kr is sensitive to the surfaces of materials in contact with the hp-gas and yields information about the surface-to-volume ratio, chemical composition,[16] and temperature[15] of the material−gas interface. The potential of hp-^{83}Kr to serve as a surface chemistry sensitive MRI contrast agent has also been demonstrated using siliconized (hydrophobic) and untreated (hydrophilic) glass surfaces.[17]

In this contribution we demonstrate that water adsorption on surfaces dramatically alters ^{83}Kr relaxation times. This effect is reversible with water desorption and is observed even for hydrophobic surfaces suggesting that hp-^{83}Kr longitudinal relaxation is potentially a powerful probe of surface hydration in systems with a wide range of surface chemistries. To test the feasibility of in vivo applications, the commercially available pulmonary surfactant extract Survanta is applied to some of the hydrated surfaces, and its influence on the ^{83}Kr T_1 time is investigated. It is shown that the range of relaxation rates can to some extent be "tuned" by adjusting krypton concentration in the krypton−helium−nitrogen optical pumping gas mixtures. Additionally, information about the presence of paramagnetic surface sites is obtained by comparing hp-^{83}Kr and hp-^{129}Xe NMR relaxation times.

Results

Probing Surfaces under Near Atmospheric Conditions. Previously, a ^{83}Kr signal enhancement of more than 3 orders of magnitude at 9.4 T field strength was obtained through RbSEOP using stopped-flow delivery. After optical pumping, the hp-gas was shuttled from the optical pumping cell to the sample contained within a pre-evacuated detection cell. Vacuum shuttling rather than the relatively slow flow often used to deliver hp-^{129}Xe is necessary because of fast quadrupolar relaxation during gas transfer.[15] However, evacuation of the sample region may alter surface hydration and is obviously ill suited for in situ and in vivo biomedical applications. Additionally, surface hydration changes may be introduced by the hp-noble gas mixtures themselves, which are devoid of water vapor due to the RbSEOP process.

Figure 1 shows an experimental apparatus that simultaneously solves both problems. The hp-gas is vacuum shuttled through pneumatic valves from the pump cell to a storage cell. Subsequently, the gas at 150−200 kPa is released into a water-filled glass container where it displaces water into an attached syringe. The gas, now at least partially saturated with water vapor, loses trace amounts of rubidium carried over from RbSEOP. Finally, the hp-gas is injected into the sample cell through operation of the syringe (see Materials and Methods). Using this procedure, the sample region is only gently ventilated by the gas flow with minimal influence on surface hydration. This procedure compared to one-step vacuum shuttling produces an acceptable hp-^{83}Kr polarization loss of at most 50%.

Of great importance for practical MR studies using hp-^{83}Kr is the magnitude of the signal intensity resulting from RbSEOP. For gas mixture I (95% Kr and 5% N_2), the ^{83}Kr polarization is typically enhanced by a factor of 1000 times that of thermal equilibrium at 9.4 T field strength, a value consistent with prior work using this gas composition.[15−18] Optical pumping of mixture II (25% Kr, 70% He, and 5% N_2) yields polarization enhancements up to 4500 times that of thermal equilibrium, which is the highest ^{83}Kr polarization enhancement yet reported in the literature. The higher polarization achieved using mixture II is probably due to reduced Rb electron spin relaxation and slower ^{83}Kr self-relaxation during the RbSEOP process. The improved spin polarization offsets the reduced spin density in the lower krypton concentration mixture. Consequently, the krypton concentration can be varied over a fairly broad range to optimized relaxational properties (see Hydrated and Dehydrated Surfaces) while maintaining comparably high signal intensities. This is demonstrated in Figure 2 where the hp-^{83}Kr NMR spectra obtained from gas mixture I and II at constant overall gas pressure yield similar integrated signal intensities.

The integrated signal intensity changes with the sample porosity and for both gas mixtures is reduced in a glass bead sample by approximately 70% compared to the detection cell without glass beads. This value corresponds well to the 74% filling factor expected for closest packing of solid spheres. Bulk magnetic susceptibility is responsible for the −1.1 ppm peak shift observed for the materials-phase (borosilicate beads) peaks compared to the peaks observed from hp-^{83}Kr in contact with the detection cell walls only. The line width is broadened from 4.5 Hz for the bulk gas-phase in the cell lacking any bead sample to 24 Hz (gas mixture I) or 16 Hz (gas mixture II) in the void spaces of the glass bead sample. The mixture dependent line width might be caused by transverse relaxational processes or coherent quadrupolar interactions on the surface,[12,14,19−25] and the magnetic susceptibility of the material leads to additional line broadening.

Hydrated and Dehydrated Surfaces. In hp-^{83}Kr magnetic resonance, the detected signal originates from gas-phase krypton but not from the adsorbed phase. However, a significant and

(9) Goodson, B. M. *J. Magn. Reson.* **2002**, *155*, 157−216.
(10) Stapf, S., Han, S. I., Eds. *Nuclear Magnetic Resonance Imaging in Chemical Engineering*; Wiley-VCH: Weinheim, Germany, 2005.
(11) Raftery, D. *Annu. Rep. NMR Spectrosc.* **2006**, *57*, 205−207.
(12) Volk, C. H.; Mark, J. G.; Grover, B. C. *Phys. Rev. A* **1979**, *20*, 2381−2388.
(13) Schaefer, S. R.; Cates, G. D.; Happer, W. *Phys. Rev. A* **1990**, *41*, 6063−6070.
(14) Butscher, R.; Wäckerle, G.; Mehring, M. *Chem. Phys. Lett.* **1996**, *249*, 444−450.
(15) Cleveland, Z. I.; Pavlovskaya, G. E.; Stupic, K. F.; LeNoir, C. F.; Meersmann, T. *J. Chem. Phys.* **2006**, *124*, 044312.
(16) Stupic, K. F.; Cleveland, Z. I.; Pavlovskaya, G. E.; Meersmann, T. *Solid State Nucl. Magn. Reson.* **2006**, *29*, 79−84.
(17) Pavlovskaya, G. E.; Cleveland, Z. I.; Stupic, K. F.; Meersmann, T. *Proc. Natl. Acad. Sci. U.S.A.* **2005**, *102*, 18275−18279.
(18) Higher polarizations have been achieved for this gas mixture in earlier work (ref 15) by using a 60 W laser system. For the relaxation measurements and NMR spectra reported in this work, a 30 W laser system is found to yield sufficiently high signal intensities.
(19) Kwon, T. M.; Mark, J. G.; Volk, C. H. *Phys. Rev. A* **1981**, *24*, 1894−1903.
(20) Raftery, D.; Long, H. W.; Shykind, D.; Grandinetti, P. J.; Pines, A. *Phys. Rev. A* **1994**, *50*, 567−574.
(21) Meersmann, T.; Smith, S. A.; Bodenhausen, G. *Phys. Rev. Lett.* **1998**, *80*, 1398−1401.
(22) Deschamps, M.; Burghardt, I.; Derouet, C.; Bodenhausen, G.; Belkic, D. *J. Chem. Phys.* **2000**, *113*, 1630−1640.
(23) Moudrakovski, I. L.; Ratcliffe, C. I.; Ripmeester, J. A. *J. Am. Chem. Soc.* **2001**, *123*, 2066−2067.
(24) Millot, Y.; Man, P. P.; Springuel-Huet, M. A.; Fraissard, J. *Stud. Surf. Sci. Catal.* **2001**, *135*.

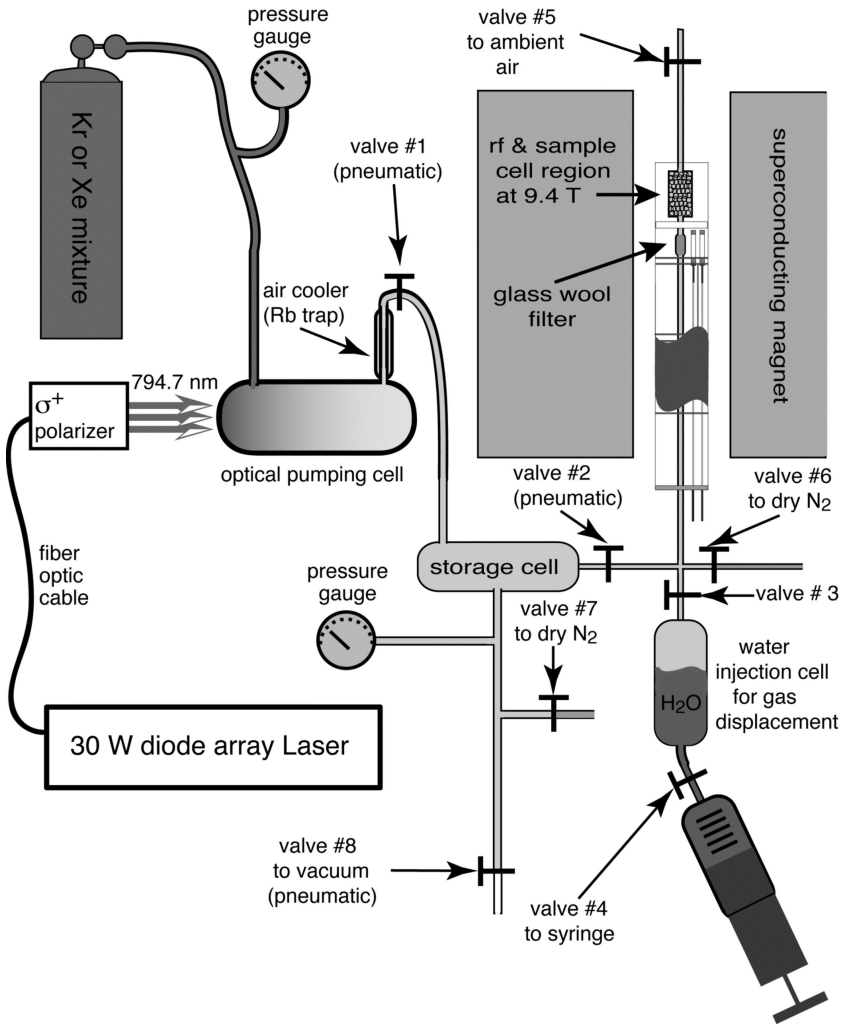

Figure 1. Apparatus for injection delivery of hp-gases. Following polarization in the optical pumping cell, hp-gas is transferred by pressure equalization to the storage cell (Valve 1 is open; valves 2, 7, and 8 are closed). Next, hp-gas is transferred to the injection cell by displacing distilled water into the syringe (Valves 2, 3, and 4 are open; valves 1, 5, 6, 7, and 8 are closed.). Finally, the hp-gas is injected into the detection region by forcing the distilled water into the injection cell (Valves 3, 4, and 5 are open; valves 2 and 6 are closed). During signal acquisition, valves 2, 3, 5, and 6 are closed to ensure constant pressure in the detection region and prevent contamination by atmospheric O_2.

often dominating contribution to the longitudinal relaxation of ^{83}Kr is caused by quadrupolar interactions during brief periods of surface adsorption. The more negative the krypton surface adsorption enthalpy, the more rapid will be the resulting surface induced relaxation. As a test system where gas-phase relaxation plays an insignificant role due to high surface-to-volume ratio, sample tubes are filled with 1 mm diameter borosilicate glass beads that allow for the study of both surface treatment[16] and hydration levels.

Figure 3 and Table 1 show how strongly the water adsorption on glass surfaces influences krypton relaxation times. At ambient pressure (85.0 kPa) and 289 K, the ^{83}Kr relaxation from gas mixture I in untreated borosilicate glass beads is prolonged by 184% from $T_1 = 22.1$ s for the dehydrated surface to $T_1 = 62.8$ s when the glass is hydrated by overnight exposure to a saturated water vapor. Similarly, a T_1 increase of 173% is observed upon hydration for mixture II. Remarkably, a dramatic increase in the longitudinal relaxation time also occurs upon hydration of a highly hydrophobic siliconized glass surface. After overnight hydration of the siliconized beads, the krypton longitudinal relaxation times experience 102% or 114% increases for mixture I and II, respectively.

The hp-^{83}Kr relaxation times in both the untreated and siliconized beads show little variation between identically treated replicate samples.[26] In fact, bead samples (both untreated and siliconized) can be thoroughly dehydrated (see Materials and Methods), subsequently placed overnight in a saturated water vapor, and then dehydrated a second time. At each stage, the resulting T_1 values are identical within experimental error to those reported in Table 1. Note that some of the data in Figure 3 do not appear to follow monoexponential behavior exactly (see for instance Figure 3A, open squares). Although the effect is not further investigated in this work, a possible explanation could be multiexponential T_1 relaxational behavior that is

(25) Meersmann, T.; Deschamps, M.; Bodenhausen, G. *J. Am. Chem. Soc.* **2001**, *123*, 941−945.

(26) Although the data in Table 1 agree qualitatively with earlier work involving similarly treated dehydrated samples (ref 16), the values in the current report are systematically lower by about 30%. The exact cause of this variation is not investigated, but a probable explanation is a difference in the average bead surface area in the two studies. The glass beads are selected for their ability to undergo surface modifying reactions and not bead-to-bead uniformity in size and shape. The beads are described as 1 mm diameter spheres; however, visual inspection reveals a distribution in the size, shape, and surface features such as corrugation and cracks.

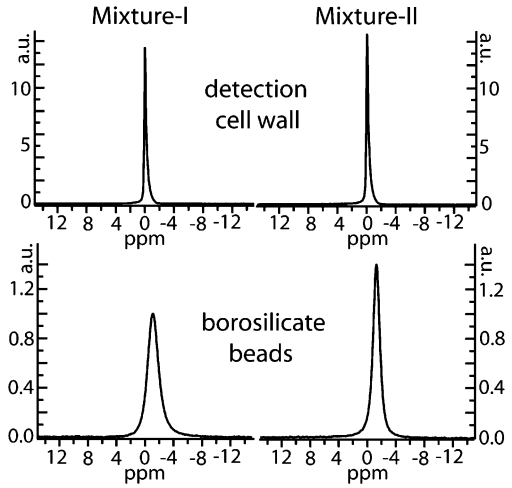

Figure 2. Hp-^{83}Kr spectra at ambient pressure. The upper two spectra are obtained from hp-^{83}Kr in contact with the detection cell wall only (without beads), and the lower spectra are obtained from hp-^{83}Kr in the cell filled with 1 mm diameter, dehydrated borosilicate glass beads. The two spectra on the left-hand side of the figure are of hp-^{83}Kr from gas mixture I (95% Kr), and the two on the right are from gas mixture II (25% Kr). All four spectra are plotted on the same arbitrary scale (a.u.) of peak height. The peak position of mixture I in the absence of borosilicate beads is used as the zero ppm reference.

possible for half-integer spins with $S > {}^1/_2$. This effect has been investigated previously by multiple quantum filtered NMR spectroscopy of dissolved metal cations such as $^{23}Na^+$ in the presence of macromolecules[27] and of ^{131}Xe in the presence of solid surfaces.[21,25]

Bovine Lung Surfactant Experiments. The ^{83}Kr longitudinal relaxation times shown in Table 2 range between approximately $T_1 = 13$ s and $T_1 = 22$ s depending on two parameters: the type of support surface used for the Survanta and the amount of water present. The label "hydrated surfactant" describes glass beads coated with undiluted Survanta without subsequent dehydration. To examine the reproducibility of the data, two trials comprising four replicate T_1 measurements each are performed and yield essentially identical results of $T_1 \approx 16$ s. Dilution, 1:2 of Survanta with distilled water, prolongs the T_1 to 21 s. Dehydration of the Survanta coated beads under vacuum conditions prolongs the T_1 to 19 s compared to that for the hydrated surfactant. An accelerated relaxation, insignificantly different from hp-^{83}Kr in contact with the hydrated, siliconized support surface without surfactant, occurs when using a Survanta coated siliconized support surface.

Hyperpolarized ^{129}Xe Relaxation Measurements. When ^{129}Xe is exposed to a glass surface, its longitudinal relaxation rate can be accelerated due to the presence of paramagnetic impurities close to the surface. This is seen in Table 3 for dehydrated glass beads with $T_1 = 43$ s, a relaxation time that is quite short for gas-phase ^{129}Xe, which in macroscopic glass containers, at near ambient pressures, and at 1.5 T can be as long as 13,200 s.[28] Hydrating the beads either obstructs xenon contact with the paramagnetic sites or reduces the overall xenon surface coverage, thus prolonging the relaxation time to $T_1 =$ 103 s. Siliconizing the surface[29−31] dramatically increases the ^{129}Xe T_1 in sharp contrast to the effect seen with krypton.[16,17] A similar effect is seen for the beads coated with lung surfactant, indicating that this treatment too obstructs a significant fraction of the paramagnetic surface sites.

Gas-Phase and Surface Contributions to ^{83}Kr Relaxation. In addition to the observed T_1 times, Tables 1 and 2 list the expected relaxation times for krypton gas mixtures extrapolated to zero pressure. In early work on gas-phase ^{83}Kr longitudinal relaxation, Brinkmann and Kuhn[32] found that the relaxation rate of krypton is linearly dependent on the krypton density. This linear dependence is due to spin-rotation interactions caused by binary krypton−krypton collisions, the frequency of which increases linearly with gas density. Their experiments were conducted at gas densities high enough to exclude surface relaxation on sample cell walls. The resulting empirical expression for the relaxation rate as a function of density was found to be

$$\frac{1}{T_1} = [(2.13 \pm 0.05) \times 10^{-3}\ \mathrm{cm^3 \cdot mol^{-1} \cdot s^{-1}}] \times \rho \quad (1)$$

where ρ is the gas density in amagat (1 amagat $= 4.4 \times 10^{-5}$ mol/cm^3).

At densities low enough for the Ideal Gas Law to apply, a linear dependence of relaxation rate upon gas pressure is expected, and it can be assumed that 1 amagat yields a pressure of approximately 100 kPa. However, in these low density and pressure regimes, wall relaxation becomes significant, and the relaxation rate takes the form

$$\frac{1}{T_1} = R_w + R_g(P) \quad (2)$$

where R_w is the wall-induced relaxation rate, which is expected to be pressure independent, and $R_g(P)$ is the pressure dependent gas-phase relaxation rate. (Note that this equation neglects a potential small pressure independent contribution due to spin-rotation coupling in bound, gas-phase ^{83}Kr−Kr van der Waals molecules.[33])

Figure 4 shows the pressure dependence of the ^{83}Kr longitudinal relaxation rate when in contact with detection cell walls only. Both mixtures display the expected linear pressure dependence and nonzero y-intercepts corresponding to R_w. Equations 3 and 4 represent linear least-square fits of the relaxation rates as a function of pressure, P, (in kPa) for gas mixture I (95% Kr) and mixture II (25% Kr), respectively.

$$\frac{1}{T_1} = [(1.79 \pm 0.02) \times 10^{-5}\ \mathrm{s^{-1}\ kPa^{-1}}] \times P + (4.5 \pm 0.1) \times 10^{-3}\ \mathrm{s^{-1}} \quad (3)$$

$$\frac{1}{T_1} = [(1.84 \pm 0.01) \times 10^{-5}\ \mathrm{s^{-1}\ kPa^{-1}}] \times P + (4.17 \pm 0.08) \times 10^{-3}\ \mathrm{s^{-1}} \quad (4)$$

(27) Jaccard, G.; Wimperis, S.; Bodenhausen, G. *J. Chem. Phys.* **1986**, *85*, 6282−6293.
(28) Pfeffer, M.; Lutz, O. *J. Magn. Reson., Ser. A* **1994**, *108*, 106−109.
(29) Driehuys, B.; Cates, G. D.; Happer, W. *Phys. Rev. Lett.* **1995**, *74*, 4943−4946.
(30) Breeze, S. R.; Lang, S.; Moudrakovski, I.; Ratcliffe, C. I.; Ripmeester, J. A.; Santyr, G.; Simard, B.; Zuger, I. *J. Appl. Phys.* **2000**, *87*, 8013−8017.
(31) Jacob, R. E.; Driehuys, B.; Saam, B. *Chem. Phys. Lett.* **2003**, *370*, 261−267.
(32) Brinkmann, D.; Kuhn, D. *Phys. Rev. A* **1980**, *21*, 163−167.
(33) Chann, B.; Nelson, I. A.; Anderson, L. W.; Driehuys, B.; Walker, T. G. *Phys. Rev. Lett.* **2002**, *88*, 113201.

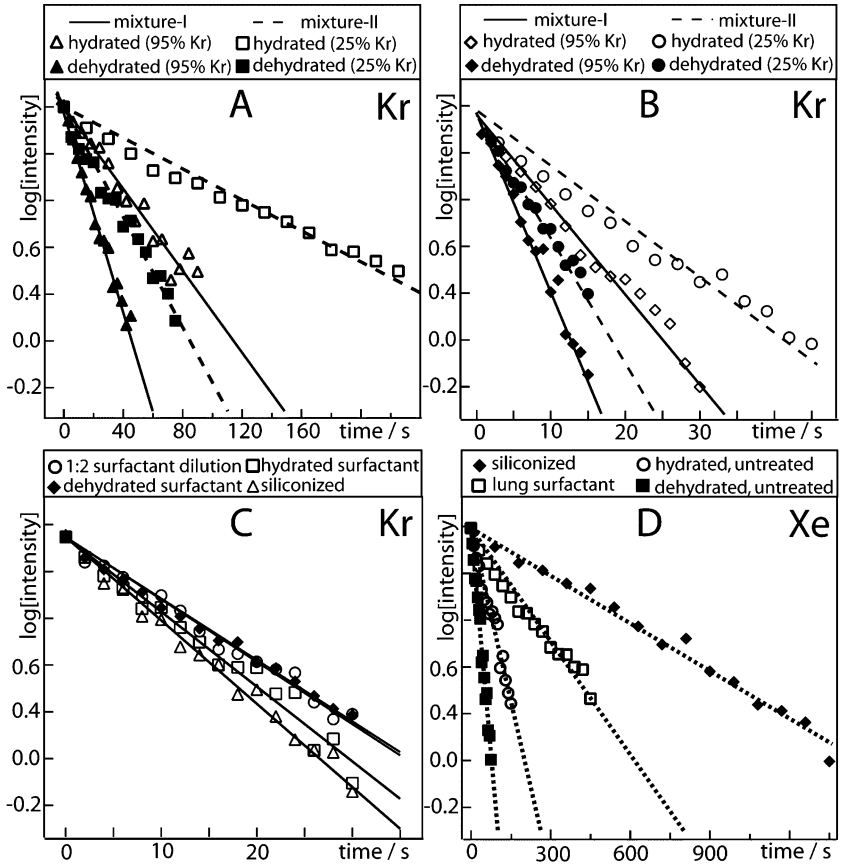

Figure 3. Signal decay of hp-^{83}Kr and hp-^{129}Xe in 1 mm borosilicate glass beads. The *y*-axes represent the log of signal intensities measured from medium angle (12°) r.f. pulses applied to single batches of hp-gas. The intensity of the first data point on each curve is scaled to the same value. The *x*-axes represent the relaxation delay times following the first r.f. pulse. Lines are linear fits of the data. Note that the T_1 values in Tables 1−3 are calculated by nonlinear least squares fitting. (A) Signal decay of hp-^{83}Kr in untreated glass beads. (B) Signal decay of hp-^{83}Kr signal in siliconized glass beads. (C) Signal decay of hp-^{83}Kr (mixture I only) in bovine lung surfactant coated beads. The label "hydrated" refers to surfactant used as supplied by the manufacturer, "dehydrated" refers to room-temperature vacuum dehydration of the surfactant, and "siliconized" refers to chemical alteration of the support surface. (D) Signal decay of hp-^{129}Xe (20% Xe) in glass beads. The label "lung surfactant" refers to surfactant used as supplied by the manufacturer.

Table 1. T_1 Values for Hp-^{83}Kr in Contact with Hydrated and Dehydrated Surfaces

	dehydrated detection cell[a,b]	hydrated detection cell[a,c]	dehydrated untreated beads[b]	hydrated untreated beads[c]	dehydrated siliconized beads[b]	hydrated siliconized beads[c]
mixture I: 95% Kr	104.3 ± 3.3 s	129.3 ± 2.8 s	22.1 ± 1.3 s	62.8 ± 3.3 s	6.1 ± 0.4 s	12.3 ± 0.5 s
mixture I: 95% Kr ($P = 0$)[d]	124.0 ± 3.6 s	161.1 ± 3.2 s	22.9 ± 1.3 s	69.5 ± 3.4 s	6.2 ± 0.4 s	12.5 ± 0.5 s
mixture II: 25% Kr	165.5 ± 3.7 s	202.3 ± 9.0 s	36.0 ± 5.5 s	98.4 ± 9.3 s	8.3 ± 0.8 s	17.8 ± 0.3 s
mixture II: 25% Kr ($P = 0$)[d]	223.4 ± 5.0 s	296.1 ± 13.5 s	38.2 ± 5.8 s	116.3 ± 10.1 s	8.4 ± 0.8 s	18.3 ± 0.3 s

[a] No bead sample present. [b] Stopped-flow delivery. [c] Injection delivery (as described in Figure 1). [d] T_1 extrapolated to zero pressure (See Gas-Phase and Surface Contributions to ^{83}Kr Relaxation).

Table 2. T_1 Values for Hp-^{83}Kr in Contact with Bovine Lung Surfactant

	hydrated (trial 1)[a]	hydrated (trail 2)[a]	1:2 dilution (surfactant/water)[a]	dehydrated[b]	hydrated (siliconized support)[a]
95% Kr	15.7 ± 0.5 s	16.2 ± 1.1 s	20.8 ± 2.1 s	19.3 ± 0.2 s	12.9 ± 0.9 s
95% Kr ($P = 0$)[c]	16.1 ± 0.5 s	16.4 ± 1.1 s	21.7 ± 2.1 s	19.9 ± 0.3 s	13.2 ± 0.9 s

[a] Injection delivery. [b] Stopped-flow delivery. [c] T_1 extrapolated to zero pressure.

Within the approximation that 1 amagat produces a pressure of 100 kPa, the slopes of these lines are in reasonably good agreement with the results of Brinkmann and Kuhn.

Although the surface area and composition of the samples determine the *y*-intercepts, the slopes of the lines depend only on the gas composition and are therefore expected to be sample independent. Thus, the value of $R_g(P)$ can be calculated and then subtracted from the observed relaxation rate. The pressure independent ($P = 0$) T_1 values in Tables 1 and 2 are calculated using the slopes from eqs 3 and 4 and exclude contributions

Table 3. T_1 Values for Hp-^{129}Xe[a] in Contact with Borosilicate Glass Beads

dehydrated untreated beads[b]	hydrated untreated beads[c]	surfactant coated beads[c]	dehydrated siliconized beads[b]
43 ± 3 s	103 ± 8 s	420 ± 27 s	773 ± 9 s

[a] 20% Xe, 5% N_2, and 70% He. [b] Stopped-flow delivery. [c] Injection delivery.

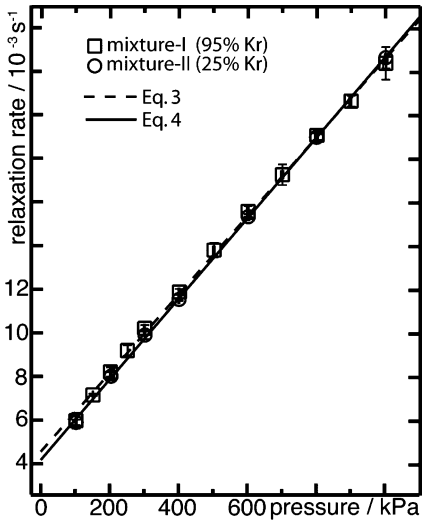

Figure 4. Pressure dependence of hp-^{83}Kr longitudinal relaxation rates. X-axis error bars represent the total pressure range contributing to each data point. The linear fits of the data and the accompanying fitting errors are presented as eq 3 (mixture I) and eq 4 (mixture II) in the text.

originating from gas-phase collisions. In the hydrated samples a small amount of water vapor is also present in the gas mixture, but its influence on the pressure dependent component of the relaxation is assumed to be negligible.

Because the surface coverage of noble gases at room temperature and near atmospheric pressure is low, gas adsorption is described by the linear portion of the Langmuir isotherm. Hence, the ratio of surface adsorbed to gas-phase krypton atoms stays constant as the pressure is moderately altered. The contribution to the relaxation arising from the surface is therefore also constant. For the surface-to-volume ratios in the studied borosilicate bead samples, the ^{83}Kr relaxation is entirely dominated by surface processes, and the data do not deviate significantly from the extrapolated zero pressure values.

Discussion

Paramagnetic Relaxation of ^{83}Kr: Comparison with Hp-^{129}Xe. Figure 5 provides a comparison of the experimental T_1 data for hp-^{83}Kr (Tables 1 and 2) and hp-^{129}Xe (Table 3). Amazingly, the ^{83}Kr relaxation times from the 25% krypton gas mixture in contact with untreated bead samples are identical within experimental error to those obtained from hp-^{129}Xe for both the dehydrated and hydrated glass surfaces. The similarity of these values is coincidental and results from the two fundamentally different relaxation mechanisms of the two noble gas isotopes. In the presence of paramagnetic surface sites, the ^{129}Xe relaxation is dominated by paramagnetic relaxation, and shielding the ^{129}Xe from these sites by siliconizing the surface increases the T_1. In contrast, the ^{83}Kr relaxation is dominated

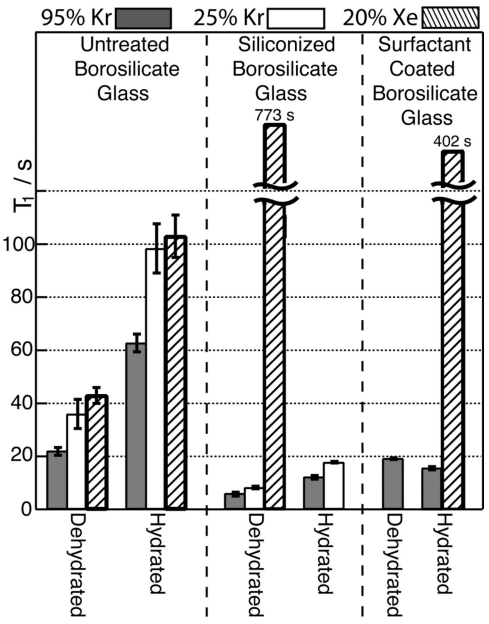

Figure 5. T_1 values of hp-^{83}Kr and hp-^{129}Xe in contact with 1 mm diameter borosilicate glass bead samples. The error bars are omitted from data for hp-^{129}Xe in contact with siliconized and surfactant coated surfaces but are reported in Table 3.

by quadrupolar contributions that increase in the presence of the nonpolar siliconized surface. The ^{83}Kr relaxation is much less affected by paramagnetic sites than the ^{129}Xe relaxation due to the 7.2 times smaller gyromagnetic ratio, γ_{Nuc}, of the ^{83}Kr nucleus, because paramagnetic relaxation follows a $T_1 \propto \gamma_{Nuc}^{-2}$ dependence.[34] The 1.9 Å van der Waals radius of krypton is only slightly smaller than the 2.2 Å radius of xenon and cannot offset the effect caused by the small γ_{Nuc} despite the $T_1 \propto r^6$ dependence on distance, r, for paramagnetically driven relaxation. However, the smaller krypton electron cloud will lead to decreased surface affinity and, therefore, to reduced contact time with the paramagnetic sites. Similar arguments explain why the presence of 20% paramagnetic gas-phase oxygen reduced the ^{83}Kr T_1 time in a desiccated canine lung specimen by only 20%.[17] The low ^{83}Kr gyromagnetic ratio, because of its inherent insensitivity to paramagnetic relaxation, can actually be advantageous for some applications of this gas, provided sufficiently high signal intensity is generated through the RbSEOP process.

Effects of Krypton Concentration on T_1 Relaxation. An important point for practical MR studies with hp-^{83}Kr is that the relaxation time in porous structures can be adjusted by changing the composition of the krypton gas mixture. Diluting the krypton leads to prolonged relaxation times, most likely because of competitive surface adsorption by the other gases in the mixture. The ^{83}Kr relaxation in porous materials is, however, relatively insensitive to changes in the total gas pressure if the surface-to-volume ratio is large enough to be the dominant source of relaxation (see Hydrated and Dehydrated Surfaces). In addition to the influence of the krypton concentration on relaxation reported here, it was previously shown that lower magnetic field strengths lead to increased ^{83}Kr relaxation rates.[15] The capability to adjust the relaxation rate by manipulating various physical interactions provides experimental adaptability

(34) Abragam, A. *The Principles of Nuclear Magnetism*; Oxford University Press: Oxford, UK, 1961.

for practical requirements such as future in vivo hp-^{83}Kr MRI for pulmonary diagnostics. For example, times substantially below 3 s would be problematic because of the duration of the inhaling process. At the other extreme, relaxation times in excess of 30 s would probably not allow for sufficient contrast because of limitations in breath holding by patients and because of competing relaxation caused by paramagnetic oxygen at prolonged timescales.

Surface Hydration. The effect of surface hydration on the ^{83}Kr longitudinal relaxation time is reminiscent of previous work with liquefied, thermally polarized ^{131}Xe (spin $S = {}^3/_2$) in aerogels where the observed relaxation times were $T_1 = 11.2$ ms (hydrated) and 3.6 ms (dehydrated).[25,35] Due to the fractal geometry of the aerogels in the 10 to 50 nm regime and the large water uptake (up to 30% of the aerogel dry weight), a substantial change in the surface morphology was the likely cause for the observed changes that also included alterations in the NMR line width and multiple quantum filtered ^{131}Xe NMR spectra.

The effect reported in this contribution is observed with gas-phase hp-^{83}Kr on glass bead surfaces with surface-to-volume ratios that are orders of magnitude smaller than that of aerogels. The ^{83}Kr relaxation time is even sensitive to water uptake on the surface of the detection cell wall (13.5 mm i.d.) in the absence of a glass beads sample (see Table 1), which has a surface-to-volume ratio approximately 2 orders of magnitude lower than that of the bead sample. Owing to this much smaller surface-to-volume ratio, gas-phase relaxation noticeably contributes to the overall relaxation time. A ^{83}Kr T_1 of 165.5 s is observed for gas mixture II at ambient pressure when in contact with a dehydrated cell wall and is prolonged by 22% to 202.3 s in contact with a hydrated cell wall. Interpolated to zero pressure, the relaxation times are $T_1 = 223.4$ s and $T_1 = 269.1$ s for the dehydrated and hydrated container walls, respectively. A similar trend is also observed for gas mixture I.

The sensitivity of hp-^{83}Kr relaxation to adsorbed surface water allows for measurements of surface hydration in a dilute gas phase at various concentrations. It also allows for measurements in systems with a wide range of low surface-to-volume ratios and small overall surface areas. A crucial result is the strong effect of water vapor on ^{83}Kr relaxation caused by siliconized (hydrophobic) surfaces. It is possible that the siliconizing of the surface is incomplete and that some untreated glass is still exposed to the gas phase. However, the long ^{129}Xe T_1 in the siliconized beads indicates that the overall glass surface exposed to the noble gases is small and that the adsorption affinity for the surface upon hydration plays an important role in extending the ^{83}Kr relaxation time.

Lung Surfactant Studies. In vivo NMR spectroscopy and MR imaging for pulmonary diagnostics are potential applications for hp-^{83}Kr because of the sensitivity of ^{83}Kr relaxation to surface chemistry in porous materials. As a model in vitro system that should be chemically similar to the interior of the mammalian pulmonary system, the commercially available bovine pulmonary extract Survanta has been selected. Survanta is used to treat premature infants with Respiratory Distress Syndrome (RDS) by lowering the surface tension on alveolar surfaces and, thus, stabilizing the alveoli against collapse. A parameter of potential importance for in vivo and in situ lung studies is the relative humidity of the gas mixture introduced. Under normal circumstances, the relative humidity inside the mammalian lung approaches 100%.[36] Even for in vitro experiments, the relative humidity is potentially important as it has been shown to influence lung surfactant adsorption kinetics at the air−water interface.[37] To minimize perturbations caused by the addition of the dry hp-gas mixtures, the injection delivery method is used for all relaxation measurements involving hydrated lung surfactant.

As a support for the bovine lung extract, 1 mm untreated and 1 mm siliconized borosilicate glass beads are selected because the void spaces formed by tightly packing the beads are similar in size to mammalian alveoli (i.e., around 200 microns in human lungs[38]). Hydrated surfactant (i.e., Survanta used as supplied by the manufacturer) appears to completely coat the glass beads and therefore strongly prolongs ^{129}Xe relaxation times (see Figure 5 and Table 3). The ^{83}Kr longitudinal relaxation time of $T_1 = 16$ s observed for krypton in the surfactant coated beads is significantly shorter than the $T_1 = 62.8$ s (mixture I) observed in untreated, hydrated glass beads. The observation of relaxation times on the order of 15 s is an important result because it suggests that similar relaxation times may be observed in vivo. Diluting the surfactant with distilled water (1:2) produces prolonged relaxation times of around $T_1 = 20$ s, perhaps due to a decreased concentration of the nonpolar surfactant components. (Note that dehydration produces a similar effect as is shown in Table 2.) The ^{83}Kr relaxation in in vivo pulmonary studies will also depend on changes in the surface-to-volume ratios since the surfactant concentration also determines the alveolar dimensions. This sensitivity to surface chemistry could be valuable for understanding certain pulmonary diseases, particularly if used in conjunction with techniques such as apparent diffusion contrast (ADC) in hp-^{3}He MRI that provide independent information about alveolar size.[39]

Conclusions

This work reports the direct comparisons of ^{129}Xe and ^{83}Kr longitudinal relaxation in porous materials. In stark contrast to ^{129}Xe, the relaxation of ^{83}Kr is largely unaffected by small amounts of paramagnetic impurities. The longitudinal nuclear spin relaxation of hyperpolarized ^{83}Kr is presented as a sensor for water adsorption on untreated, hydrophilic and siliconized, strongly hydrophobic glass surfaces. The method does not require vacuum conditions or optical transparency and allows for measurements under near atmospheric conditions in systems with low surface-to-volume ratios.

Surfaces coated with bovine pulmonary extract produce ^{83}Kr T_1 times that are of reasonable lengths for medical applications and sensitive to changes in the chemical composition of the surfactant. The results are promising for future in vivo hp-^{83}Kr MRI diagnosis of various forms of acute lung injury (ALI), including the most severe form, acute respiratory distress

(35) Pavlovskaya, G.; Blue, A. K.; Gibbs, S. J.; Haake, M.; Cros, F.; Malier, L.; Meersmann, T. *J. Magn. Reson.* **1999**, *137*, 258−264.
(36) Schmidt-Nielsen, K. *Animal Physiology: Adaptation and Environment*, 5th ed.; Cambridge University Press: Cambridge, UK, 1997.
(37) Zuo, Y. Y.; Gitiafroz, R.; Acosta, E.; Policova, Z.; Cox, P. N.; Hair, M. L.; Neumann, A. W. *Langmuir* **2005**, *21*, 10593−10601.
(38) Ochs, M.; Nyengaard, L. R.; Jung, A.; Knudsen, L.; Voigt, M.; Wahlers, T.; Richter, J.; Gundersen, H. J. G. *Am. J. Resp. Crit. Care* **2004**, *169*, 120−124.
(39) Yablonskiy, D. A.; Sukstanskii, A. L.; Leawoods, J. C.; Gierada, D. S.; Bretthorst, G. L.; Lefrak, S. S.; Cooper, J. D.; Conradi, M. S. *Proc. Natl. Acad. Sci. U.S.A.* **2002**, *99*, 3111−3116.

syndrome (ARDS),[40] which are characterized by alteration in the lipid and protein composition of the pulmonary surfactant system,[41,42] alveolar fluid levels,[43] and alveolar size.[44] The longitudinal relaxation of hp-^{83}Kr is, in principle, sensitive to all of these changes and, in concert with biochemical and biophysical markers,[45] could provide a powerful tool for early diagnosis of ALI in at risk individuals, monitoring the effectiveness of ALI therapies, and developing improved surfactant therapies.[46]

Future work will focus on evaluating the ability of hp-^{83}Kr to detect chemical changes in the adsorbed surface water (e.g., effective pH and ionic strength). Additionally, materials science applications will need to focus on quantifying water uptake on various materials, comparing krypton relaxation data with more traditional measures of macroscopic surface wettability[47,48] such as contact angle measurements with sessile water droplets, and examining the influence of alternate adsorbing molecules (e.g., short chain alcohols) on relaxation. Potential applications of this technique are the water content analysis of solid chemicals, pharmaceutical products, and food materials that otherwise rely on Karl Fischer water titrations that can be complicated by side reactions and reagent instability.[49] In situ hp-^{83}Kr MR imaging could also potentially monitor the water distribution in porous fuel cell cathodes that require careful engineering of composite hydrophobic and hydrophilic surface sites to allow optimized water transport without flooding.[50]

As a final point, it is also demonstrated that the hp-^{83}Kr relaxation is dependent on the krypton concentration in the gas mixtures used. This allows for optimizing the range of the relaxation times for particular applications. For a reasonably broad range of gas compositions, this ability to tune the relaxational properties of the gas mixture can be achieved without sacrificing signal intensity.

Materials and Methods

NMR Measurements and Instrumentation. Experiments are performed on a Chemagnetics CMX II 400 MHz NMR spectrometer in a 9.4 T wide-bore (89 mm) superconducting magnet. All NMR data are obtained at a temperature of approximately 290 K using custom-built, gas-flow probes tuned to the frequency of either ^{83}Kr (15.4 MHz) or ^{129}Xe (110.6 MHz). T_1 values from hp-gases are calculated by nonlinear least-squares fitting of the NMR signal as a function of time and number of applied medium flip angle (~12°) r.f. pulses. The 90° pulses for ^{83}Kr (63μs) and ^{129}Xe (47μs) are determined under continuous-flow optical pumping conditions similar to those used in earlier work.[15,51] All T_1 values reported are the averages of four to eight replicate measurements and, unless otherwise indicated, are conducted at 85.0 ± 0.5 kPa (i.e., ambient pressure at the laboratory elevation of 1500 m). The errors reported are the standard deviations resulting from those replicate measurements. The signal enhancements reported for hp-^{83}Kr are referenced to the thermal signal obtained from a sample containing 500 kPa natural abundance Kr and 100 kPa O_2.

Optical Pumping of ^{83}Kr and ^{129}Xe. All gas mixtures in this work are produced from research grade krypton (99.995%, natural abundance), xenon (99.995%, natural abundance), nitrogen (99.9997%), and helium (99.9999%) (Airgas, Radnor, PA). Optical pumping is performed in a cylindrical Pyrex cell (length = 125 mm, i.d. = 24 mm). The gas mixtures consist of 95% Kr and 5% N_2 (mixture I); 25% Kr, 5% N_2, and 70% He (mixture II); or 20% Xe, 5% N_2, and 75% He. N_2 is added to the mixtures for radiation quenching purposes.[51] The pump cell, containing approximately 1 g of rubidium (99.75%; Alfa Aesar, Ward Hill, MA), is housed in a quartz and aluminum oven to maintain even heating (438 ± 5 K for ^{83}Kr and 393 ± 5 K for ^{129}Xe). The pump cell is maintained above ambient pressure (150−200 kPa) to avoid pump cell contamination. Light (794.7 nm) from a 30 W Coherent FAP diode-array laser system (line width 2 nm) is directed via fiber optic coupling cables through a circular polarizer onto the pumping cell. After the light passes through the fiber optics and the polarizer, the power is reduced to approximately 20 W. The magnetic field needed for RbSEOP is provided by the fringe field of the superconducting magnet (0.05 T). Rb vapor is separated from the hp-gas mixtures by an air-cooled trap at the outlet to the pump cell and a glass wool filter placed directly before the sample region.

Delivery of Optically Pumped Gases. In the stopped-flow experiments with ^{83}Kr used to measure T_1 values in the dehydrated samples, polarization is allowed to build for several minutes in the pump cell. During this time the detection cell (length = 50 mm, i.d = 12 mm) is evacuated to less than 0.1 kPa. Following polarization, the hp-gas is rapidly transferred from the pump cell to the detection cell by pressure equalization. In the injection delivery method (see Figure 1), polarizations build for several minutes and then the hp-gas mixture is transferred by pressure equalization into an evacuated Pyrex storage cell (length = 80 mm, i.d. = 24 mm). From the storage cell, the hp-gas mixture is transferred to a Pyrex injection cell (length = 150 mm, i.d. = 24 mm) containing distilled water and a thermally polarized gas mixture having the same composition as that of the hp-gas mixture. During this transfer from the storage cell, approximately 50 mL of distilled water is displaced into the attached syringe. The syringe then forces the distilled water back into the injection cell and, thus, the hp-gas mixture into the sample region for detection. To limit the exposure of hp-gases to O_2, He gas is bubbled through the water in the injection cell for several minutes prior to conducting injection delivery experiments. The apparatus is then thoroughly flushed with nitrogen gas prior to filling the injection and detection cells with the thermally polarized noble gas mixture. Between experiments, the storage cell is repeatedly filled with dry N_2 and evacuated to reduce pump cell contamination by water vapor.

Preparation of Borosilicate Glass Beads. Untreated, 1.0 mm diameter, borosilicate glass beads (Biospec Products, Inc., Bartlesville, OK) are degassed overnight at a temperature of 473 K and a pressure of less than 0.1 Pa and then stored under dry nitrogen until use (stopped-flow delivery) or stored overnight in a saturated water vapor (injection delivery). Siliconized beads are prepared as described elsewhere.[16,17] Following surface treatment, the siliconized beads are hydrated or dehydrated using the same procedure as that used for the untreated beads.

Storage and Application of Lung Surfactant. A 4 mL vial of Survanta (Ross Products Division, Abbott Laboratories, Columbus, OH), a suspension of bovine pulmonary surfactant extract, is stored under refrigerated conditions in accordance with the manufacturer's instructions prior to use. The chemical composition of Survanta (as stated by the manufacturer) is primarily that of natural bovine lung extract and comprises phospholipids (25 mg/mL), triglycerides (0.5−1.75 mg/mL), free fatty acids (1.4−3.5 mg/mL), and surfactant associated proteins (>1 mg/mL) suspended in a 0.9% aqueous NaCl solution. Before applying the suspension to the various bead samples,

(40) Repine, J. E. *Lancet* **1992**, *339*, 466−469.
(41) Schmidt, R.; Meier, U.; Yabut-Perez, M.; Walmrath, D.; Grimminger, F.; Seeger, W.; Gunther, A. *Am. J. Resp. Crit. Care* **2001**, *163*, 95−100.
(42) Cochrane, C. G. *Am. J. Physiol. Lung Cell. Mol. Physiol.* **2005**, *288*, L608−L609.
(43) Guidot, D. M.; Folkesson, H. G.; Jain, L.; Sznajder, J. I.; Pittet, J.-F.; Matthay, M. A. *Am. J. Physiol. Lung Cell. Mol. Physiol.* **2006**, *291*, L301−L306.
(44) Schiller, H. J.; McCann, U. G.; Carney, D. E.; Gatto, L. A.; Steinberg, J. M.; Nieman, G. F. *Crit. Care Med.* **2001**, *29*, 1049−1055.
(45) Connelly, K. G.; Repine, J. E. *Annu. Rev. Med.* **1997**, *48*, 429−445.
(46) Cochrane, C. G.; Revak, S. D. *Chest* **1999**, *116*, 85S-86S.
(47) Adamson, A. W.; Gast, A. P. *Physical Chemistry of Surfaces*; John Wiley & Sons, Inc.: New York, 1997.
(48) Fuji, M.; Fujimori, H.; Takei, T.; Watanabe, T.; Chikazawa, M. *J. Phys. Chem. B* **1998**, *102*, 10498−10504.
(49) Grunke, S. *Food Control* **2001**, *12*, 419−426.
(50) Zhang, F. Y.; Yang, X. G.; Wang, C. Y. *J. Electrochem. Soc.* **2006**, *153*, A225−A232.
(51) Mortuza, M. G.; Anala, S.; Pavlovskaya, G. E.; Dieken, T. J.; Meersmann, T. *J. Chem. Phys.* **2003**, *118*, 1581−1584.

Survanta is removed from refrigeration and warmed to room temperature. A sterile syringe is then used to remove a portion of the suspension through a rubber septum. The beads are coated with approximately 0.3 mL of Survanta by gently rolling the beads in a few droplets of surfactant mixture until the glass surface is visibly covered. For one sample, the surfactant extract is diluted 1:2 with distilled water but, otherwise, treated identically. For the dehydrated lung surfactant sample, untreated beads are coated in an identical manner to that used for the hydrated samples, transferred to the detection cell, and dried overnight at room temperature under a 0.1 Pa vacuum.

Acknowledgment. This material is based upon work supported by the National Science Foundation under Grant No. CHE-0135082. The authors wish to thank Michael D. Olsen for constructing the specialized glassware used in this work, Dr. David W. Grainger for stimulating discussions, Nancy D. Elkins for advise involving the Survanta bovine lung extract, and Ramon A. Saavedra for assisting with the hyperpolarized krypton relaxation measurements.

JA065994T